4D-Flow MRI of aortic and valvular disease

Juffermans, J.F.

PART 1.

Reproducibility and Consistency

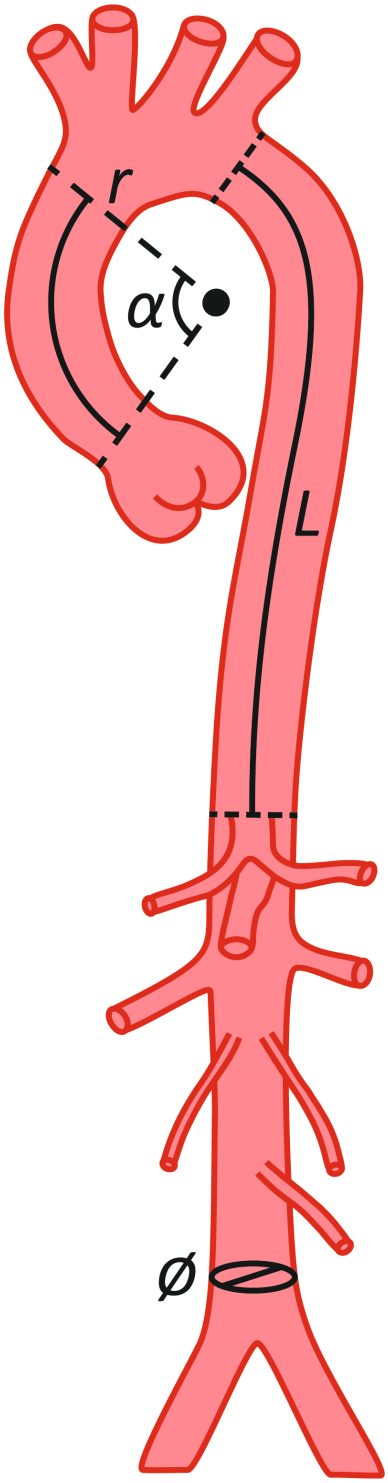
r
α
L
ø

CHAPTER 2

Reproducibility of Aorta Segmentation on 4D Flow MRI in Healthy Volunteers

Joe F. Juffermans, Jos J.M. Westenberg, Pieter J. van den Boogaard, Arno A.W. Roest, Hans C. van Assen, Roel L.F. van der Palen, and Hildo J. Lamb

JOURNAL OF MAGNETIC RESONANCE IMAGING, 2021, 53.4: 1268-1279.

ABSTRACT

Background: Hemodynamic aorta parameters can be derived from 4D flow MRI, but this requires lumen segmentation. In both commercially available and research 4D flow MRI software tools, lumen segmentation is mostly (semi-)automatically performed and subsequently manually improved by an observer. Since the segmentation variability, together with 4D flow MRI data and image processing algorithms, will contribute to the reproducibility of patient-specific flow properties, the observer's lumen segmentation reproducibility and repeatability needs to be assessed.

Purpose: To determine the interexamination, interobserver reproducibility, and intraobserver repeatability of aortic lumen segmentation on 4D flow MRI.

Study Type: Prospective and retrospective.

Population: A healthy volunteer cohort of 10 subjects who underwent 4D flow MRI twice. Also, a clinical cohort of six subjects who underwent 4D flow MRI once.

Field Strength/Sequence: 3T; time-resolved three-directional and 3D velocity-encoded sequence (4D flow MRI).

Assessment: The thoracic aorta was segmented on the 4D flow MRI in five systolic phases. By positioning six planes perpendicular to a segmentation's centerline, the aorta was divided into five segments. The volume, surface area, centerline length, maximal diameter, and curvature radius were determined for each segment.

Statistical Tests: To assess the reproducibility, the coefficient of variation (COV), Pearson correlation coefficient (r), and intraclass correlation coefficient (ICC) were calculated.

Results: The interexamination and interobserver reproducibility and intraobserver repeatability were comparable for each parameter. For both cohorts there was very good reproducibility and repeatability for volume, surface area, and centerline length (COV = 10–32%, r = 0.54–0.95 and ICC = 0.65–0.99), excellent reproducibility and repeatability for maximal diameter (COV = 3–11%, r = 0.94–0.99, ICC = 0.94–0.99), and good reproducibility and repeatability for curvature radius (COV = 25–62%, r = 0.73–0.95, ICC = 0.84–0.97).

Data Conclusion: This study demonstrated no major reproducibility and repeatability limitations for 4D flow MRI aortic lumen segmentation.

INTRODUCTION

Four-dimensional (4D) flow MRI, also known as time-resolved three-directional and three-dimensional velocity-encoded MRI or phase-contrast MRI, is an imaging modality that is used to analyze aortic flow hemodynamics. With 4D flow MRI, multiple patient-specific flow properties can be quantified, such as the wall shear stress [1-3]. It has been hypothesized that changes in wall shear stress may affect endothelium properties within the vessel wall [4], which may promote vascular dilation and remodeling [5].

For the numerical calculation of the 4D flow MRI derived hemodynamic parameters, a cardiac phase specific 3D lumen segmentation of the aorta is required [3, 6]. In both commercially available and research 4D flow MRI software tools, lumen segmentation is mostly (semi-)automatically performed and subsequently manually improved by an observer. Therefore, the observer's lumen interpretation may lead to segmentation variability [2, 3, 7, 8]. The aortic lumen segmentation reproducibility was not assessed in previous studies which evaluated the reproducibility of several 4D flow MRI derived hemodynamic parameters [8-12]. Since the segmentation variability, together with 4D flow MRI data and image processing algorithms, contributes to the reproducibility of patient-specific flow properties [6], the observer's lumen segmentation reproducibility and repeatability needs to be assessed.

Furthermore, the aortic lumen segmentation could be used to automatically derive several morphological parameters, like the maximal vessel diameter. Clinical guidelines recommend measurement of maximal diameter perpendicular to the vessel longitudinal axis for the highest reproducibility [13, 14]. This recommendation is challenging for observers, since they have to manually determine the optimal plane location and angulation towards the vessel [15]. These difficulties could potentially be minimized by automatically deriving the maximal diameter from a lumen segmentation. However, as a result of the unknown lumen segmentation reproducibility, it remains uncertain if the automatically derived maximal diameter could be used to accurately describe patient characteristics. This information is especially important for the clinical follow-up of patients with aorta pathologies, such as aneurysms or coarctations [13, 14].

Therefore, the purpose of this study was to determine: 1) interexamination, 2) interobserver reproducibility, and 3) intraobserver repeatability of aortic lumen segmentation on 4D flow MRI.

MATERIALS AND METHODS

Study Population

This study protocol was approved by the Medical Ethics Committee of the Leiden University Medical Center and written informed consent was obtained from all subjects.

The interexamination reproducibility and intraobserver repeatability was assessed in a healthy volunteer cohort, and the interobserver reproducibility was assessed in a healthy volunteer cohort and a clinically relevant cohort. The prospective included a healthy cohort consisting of 10 healthy volunteers (27 ± 3 years, 50% male) without a history of cardiovascular disease who underwent two 4D flow MRI examinations between July 2015 and March 2017. These examinations were planned consecutively with a 10-minute break between them and included repositioning and replanning of all subjects. The retrospective included a clinical cohort consisting of two patients after surgical coarctation repair (13 ± 1 years, one male and one female, one with a restenosis, and one with a bicuspid aortic valve), two aneurysm patients (65 ± 8 years, one male and one female), and two older healthy volunteers (59 ± 5 years, one male and one female) who underwent a 4D flow MRI examination between September 2015 and November 2019. The data from 10 of the 10 subjects of the healthy volunteer cohort has been previously reported [10] in a prior article that assessed the interexamination, interobserver, and intraobserver reproducibility of 3D wall shear stress in the thoracic aorta.

MRI Acquisition

The MRI examination consisted of a 4D flow MRI sequence incorporating the thoracic aorta from the aortic valve to descending aorta at the level of the diaphragm. For the MRI sequence parameters, see Table 1. All subjects were scanned with a 3T scanner (Ingenia, Philips Medical Systems, Best, The Netherlands) using a FlexCoverage anterior and dStream Torso posterior coil. Concomitant gradient correction and local phase correction were performed using standard available scanner software.

Table 1. The MRI sequence parameters.

Parameter	4D flow MRI
Respiratory compensation	Hemidiaphragm respiratory navigator
Electrocardiographic gating	retrospective
Field of view [mm^3]	350 x 250 x 75
Acquired spatial resolution [mm^3]	2.5 x 2.5 x 2.5
Temporal resolution [ms]	35.1 – 36.5
Echo time [ms]	2.5 – 2.7
Repetition time [ms]	4.4 – 4.6
Flip angle [degree]	10
Planned acquisition time* [seconds]	403 ± 35
Turbo field echo	2
Acceleration method	SENSE 2.5 in anterior-posterior direction
Velocity encoding gradient [cm/s]	200

Data notated as the mean ± standard deviation. * - excluding hemidiaphragm respiratory navigator.

Image Analysis

The image analysis consisted of two parts to derive the aorta morphology. First, the thoracic aorta lumen was segmented between the aortic valve and the descending aorta, excluding the subclavian and carotid arteries. The aortas of the healthy cohort were segmented twice by the first observer (R.P. with 6 years 4D flow MRI experience) on the first 4D flow MRI, once by the first observer on the second 4D flow MRI, and once by the second and third observers (P.B. and J.J. with 12 and 3 years 4D flow MRI experience, respectively) on the first 4D flow MRI. The aortas of the clinical cohort were segmented once by the first, second, and third observer. The interobserver analysis between the first and second, first and third, and second and third observers are numbered 1, 2, and 3, respectively.

The 4D flow segmentation was performed from a combined weighted magnitude and velocity image with CAAS MR 4D Flow v1.1 and CAAS MR Solutions v5.1 (Pie Medical Imaging, Maastricht, The Netherlands). Utilizing CAAS software, the peak systolic phase and two consecutive phases before and two after this peak systolic phase were segmented. By manually placing start and endpoints in the aorta, a lumen segmentation was automatically created, which subsequently was manually improved for each phase. Next, the thoracic aortic lumen was divided into five consecutive segments by manually placing anatomical planes perpendicular to the aortic centerline: the proximal ascending aorta (from the sinotubular junction to the mid-ascending aorta), distal ascending aorta (from the midascending aorta to the brachiocephalic artery), aortic arch (from the brachiocephalic artery up and including the left subclavian artery), proximal descending aorta (from the left subclavian artery to the mid-descending thoracic aorta), and distal descending aorta (from the mid-descending thoracic aorta to the descending aorta at the level of the aortic valve, Figure 1). For the clinical cohort, the image analysis required ±30 minutes to segment and partition the aorta for the five systolic phases per subject per observer. In total, the aortas of the 16 subjects were segmented at five different cardiac phases and then partitioned into five anatomical segments resulting in a total of 1700 individual anatomical aortic lumen segments. The aorta segmentation is described in more detail by Van der Palen et al [10].

Next, the morphometry of the aorta segmentation was fully automatically processed using in-house developed Python v3.6.4 (Python Software Foundation, Wilmington, DE) software [16-19]. For each anatomical segment, the volume, surface area, centerline length, maximal diameter, and the curvature radius (longitudinal bending radius) were computed. The maximal diameter was derived by first constructing a perpendicular plane to the centerline every millimeter. Next, the cross-sectional lumen areas between the perpendicular planes and the lumen segmentation were used to derive the lumen diameter, assuming a circular lumen area. The curvature radius was derived by first finding the best-fitting plane to the segment's centerline. Next, the centerline points were projected on the fitting plane and a circle was fitted through them (see Figure 1). To determine the accuracy of the in-house-developed tool, synthesized and 4D flow MRI phantom data were investigated (see Appendix).

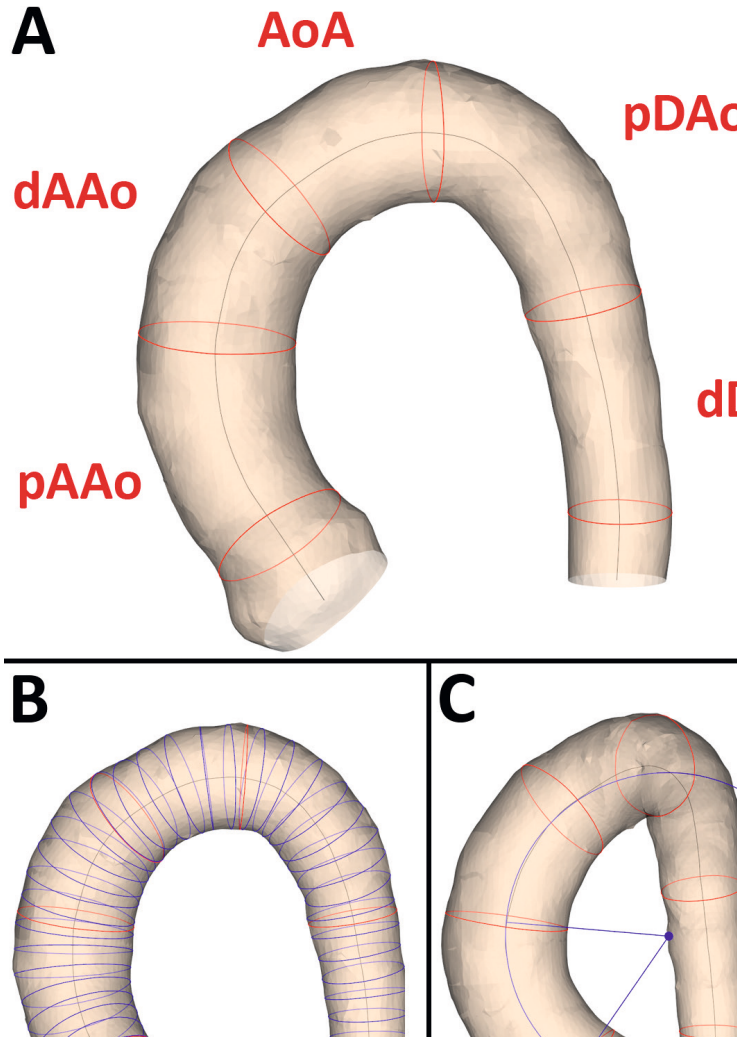

FIGURE 1. The aortic lumen segmentation with (a) the anatomical segments, (b) the lumen cross-section to derive maximal diameter, (c) and a circle fitted to the proximal ascending aorta. Example of an aorta lumen segmentation of a healthy volunteer. (a) The anatomical segments. (b) The crosssections to derive the lumen diameter. To improve visibility, the cross-sections are displayed every 5 mm instead of every mm that was used during the analysis. (c) A circle fitted to the proximal ascending aorta. pAAo = proximal ascending aorta (from the sinotubular junction to the mid-ascending aorta), dAAo = distal ascending aorta (from the mid-ascending aorta to the brachiocephalic artery), AoA = aortic arch (from the brachiocephalic artery up and including the left subclavian artery), pDAo = proximal descending aorta (from the left subclavian artery to the mid-descending thoracic aorta) and dDAo = distal descending (from the mid-descending thoracic aorta to the descending aorta at the level of the aortic valve).

Statistical analysis

The statistical analysis of the, interexamination, interobserver reproducibility, and intraobserver repeatability was performed using the SPSS v23 software (IBM, Armonk, NY). All continuous parameters were expressed as the mean with standard deviation (mean ± standard deviation). The characteristic differences within the healthy subject cohort were evaluated with paired t-tests. To assess reproducibility, Bland–Altman analysis [20], coefficients of variation (COV), Pearson correlation coefficients (r), and intraclass correlation coefficients (ICC) were calculated. For the Bland–Altman analysis the mean difference (Diff) and limits of agreement (LoA; ±1.96 standard deviation of Diff) were computed. The COV was classified as: low (≤10%), intermediate (11–20%), high (21–30%), and very high (>30%). The r and ICC were classified as: poor (<0.50), moderate (0.50–0.69), good (0.70–0.84), very good (0.85–0.94), and excellent (≥0.95). $P < 0.05$ was considered statistically significant.

RESULTS

The baseline characteristics of the healthy volunteers and clinical cohort are shown in Table 2. Between the first and second examinations, the healthy volunteer cohort had no significant differences in heart rate (61 ± 8 vs. 62 ± 6 bpm, p = 0.65) and trigger delays for the five systolic phases (p = 0.91, 0.86, 0.85, 0.83, and 0.83, respectively, for phases one to five). The phantom analysis demonstrated that the aorta morphometry can be derived from a lumen segmentation with a very-low (<5%) relative error by the in-house-developed software tool (see Appendix). The morphometric baseline characteristics derived from the first 4D flow MRI of all subjects are displayed in Table 3.

The interexamination, interobserver reproducibility, and intraobserver repeatability results of the healthy cohort over all subjects, anatomical segments, and cardiac phases are presented in Table 4. In general, for the healthy cohort the analysis demonstrated a very good reproducibility and repeatability for volume, surface area, and centerline length (COV = 10–21%, r = 0.54–0.92 and ICC = 0.65–0.96), excellent reproducibility and repeatability for maximal diameter (COV = 3–4%, r = 0.96–0.97, ICC = 0.94–0.99), and good reproducibility and repeatability for curvature radius (COV = 44–62%, r = 0.73–0.89, ICC = 0.84–0.92). The Bland–Altman plots (Figures 2–6) demonstrated LoAs equal to or smaller than: volume 4.5 mL, surface area 7.3 mm^2 , centerline length 10.3 mm, maximal diameter 2.0 mm, and curvature radius 68.0 mm.

Table 2. The study population and 4D flow MRI characteristics.

	Healthy cohort				Clinical cohort		
	Volunteers	**First 4D flow MRI**	**Second 4D flow MRI**	**Probability value paired t-test**	**Coarctation patients**	**Aneurysm patients**	**Healthy volunteers**
Population size	10				2	2	2
Male (%)	5 (50%)				1 (50%)	1 (50%)	1 (50%)
Age [years]	26.5 ± 2.6				13.0 ± 1.4	64.5 ± 7.8	58.5 ± 4.9
Height [cm]	176 ± 7				151 ± 14	181 ± 9	180 ± 1
Weight [kg]	68 ± 3				38 ± 8	80 ± 1	73 ± 16
BSA [m^2]	1.8 ± 0.2				1.3 ± 0.2	2.0 ± 0.1	1.9 ± 0.2
Heart rate [bpm]		61 ± 8	62 ± 6	0.65	77 ± 18	62 ± 15	64 ± 10
Trigger delay peak systole -2 phases [ms]		104 ± 19	103 ± 19	0.91	122 ± 23	110 ± 38	91 ± 47
Trigger delay peak systole -1 phases [ms]		137 ± 18.4	135 ± 18	0.86	149 ±25	142 ± 43	120 ± 47
Trigger delay peak systole [ms]		169 ± 18	168 ± 18	0.85	175 ± 25	172 ± 48	149 ± 51
Trigger delay peak systole +1 phases [ms]		202 ± 18	200 ± 17	0.83	202 ± 27	203 ± 52	179 ± 52
Trigger delay peak systole +2 phases [ms]		234 ± 18	232 ± 17	0.83	229 ± 28	235 ± 57	209 ± 54

Data notated as the mean ± standard deviation. Abbreviations: BSA – body surface area according to the DuBois formula and bpm – beats per minute.

Table 3. The morphometric characteristics of study population.

Seg	Cohort	Subgroup	Volume [mL]	Surface area [cm^2]	Centerline length [mm]	Maximal diameter [mm]	Curvature radius [mm]
pAAo	Healthy	Volunteer	13.6 ± 3.2	22.6 ± 3.9	28.8 ± 4.0	25.7 ± 2.1	33.1 ± 6.3
	Clinical	CoA	11.7 ± 1.6	21.8 ± 0.9	31.9 ± 2.1	24.5 ± 3.7	35.5 ± 5.5
		TAA	49.1 ± 17.1	51.5 ± 14.7	41.8 ± 9.2	42.1 ± 3.8	44.5 ± 3.3
		Volunteer	29.6 ± 10.0	35.2 ± 15.9	45.9 ± 4.6	31.2 ± 4.5	69.2 ± 3.5
dAAo	Healthy	Volunteer	12.7 ± 3.1	20.5 ± 3.7	25.9 ± 3.7	25.7 ± 2.0	37.6 ± 8.4
	Clinical	CoA	9.5 ± 1.1	19.0 ± 1.3	30.1 ± 0.6	21.3 ± 0.3	47.8 ± 17.7
		TAA	50.7 ± 16.8	53.6 ± 15.8	44.6 ± 11.4	41.8 ± 3.8	46.8 ± 13.9
		Volunteer	36.1 ± 12.4	40.1 ± 16.5	46.5 ± 4.6	31.7 ± 4.2	36.1 ± 3.0
AoA	Healthy	Volunteer	12.8 ± 4.1	22.8 ± 5.5	31.3 ± 5.5	24.3 ± 2.0	30.0 ± 8.1
	Clinical	CoA	4.2 ± 1.2	9.9 ± 1.6	18.1 ± 1.1	18.5 ± 2.1	13.3 ± 2.6
		TAA	29.4 ± 1.6	40.3 ± 0.9	43.4 ± 0.3	34.0 ± 0.2	80.6 ± 29.4
		Volunteer	21.0 ± 6.6	27.2 ± 13.1	37.8 ± 7.4	28.9 ± 3.1	59.5 ± 3.1
pDAo	Healthy	Volunteer	10.6 ± 2.6	21.5 ± 4.1	34.3 ± 5.9	21.4 ± 1.8	30.3 ± 5.5
	Clinical	CoA	5.0 ± 0.2	14.2 ± 1.1	31.4 ± 3.8	15.8 ± 1.2	56.4 ± 19.6
		TAA	35.5 ± 0.3	52.0 ± 2.8	58.6 ± 7.8	30.5 ± 3.2	33.3 ± 13.0
		Volunteer	29.7 ± 3.4	39.0 ± 13.1	58.9 ± 4.7	26.5 ± 0.1	35.4 ± 1.5
dDAo	Healthy	Volunteer	8.7 ± 2.0	18.8 ± 2.7	32.1 ± 3.8	19.5 ± 2.2	107.7 ± 49.7
	Clinical	CoA	5.3 ± 1.0	14.7 ± 2.4	32.1 ± 4.6	15.0 ± 0.3	93.5 ± 8.4
		TAA	24.1 ± 3.3	42.2 ± 5.6	58.4 ± 7.7	24.8 ± 0.5	102.4 ± 36.5
		Volunteer	25.8 ± 4.5	35.0 ± 14.2	57.1 ± 4.9	24.7 ± 1.2	196.8 ± 32.9

Characteristics are presented per cohort and subgroup over all cardiac phases and expressed as the mean ± standard deviation. Abbreviations: CoA – coarctation patient, TAA – thoracic ascending aneurysm patient, pAAo – proximal ascending aorta, dAAo – distal ascending aorta, AoA – Aortic arch, pDAo – proximal descending aorta, dDAo – distal descending aorta and Seg – Segmentation.

The interexamination, interobserver reproducibility, and intraobserver repeatability results of the healthy cohort per anatomical segment are presented in Supplemental Tables S1, S2, and S3, respectively. These results showed a comparable reproducibility and repeatability per anatomical segment for most parameters. However, the volume, surface area, and centerline length reproducibility and repeatability were decreased for the proximal ascending aorta (pAAo). The curvature radius reproducibility was decreased for the distal descending aorta (dDAo) (LoA = 90.6–130.9 mm) compared with the other anatomical segments (LoA = 4.7–23.5 mm).

The interobserver reproducibility results of the clinical cohort over all subjects, anatomical segments, and cardiac phases are presented in Table 5. In general, for the clinical cohort the analysis demonstrated a very good reproducibility for volume, surface area, centerline length, and curvature radius (COV = 10–41%, r = 0.83–0.95, ICC = 0.91–0.99) and excellent reproducibility for maximal diameter (COV = 4–11%, r = 0.94–0.99, ICC = 0.97–0.99). The Bland–Altman analysis demonstrated LoAs equal to or smaller than: volume 14.9 mL, surface area 18.9 mm^2, centerline length 13.1 mm, maximal diameter 5.8 mm, and curvature radius 54.9 mm.

The interobserver results of the clinical cohort per subgroup are presented in Supplemental Table S4. These results showed a comparable reproducibility per subgroup.

DISCUSSION

In this study the interexamination, interobserver reproducibility, and intraobserver repeatability of aortic lumen segmentation on 4D flow MRI was evaluated in a healthy subject and clinically relevant cohort. The main findings of this study were as follows: 1) The interexamination, interobserver, and intraobserver analysis demonstrated a very good aortic lumen segmentation reproducibility and repeatability. 2) The analysis demonstrated an excellent reproducibility and repeatability for assessment of the maximal diameter. 3) The analysis demonstrated slightly larger, but still acceptable, LoAs for the clinical cohort compared to the healthy cohort.

The interexamination, interobserver, and intraobserver analysis demonstrated comparable reproducibility and repeatability or each parameter for both cohorts. Comparable interobserver reproducibility and intraobserver repeatability have previously been described for volume, centerline length, maximal diameter, and curvature radius in studies analyzing nonelectrocardiographic-gated contrast-enhanced MRI, 4D flow MRI, and computed tomography images in patients [21-25].

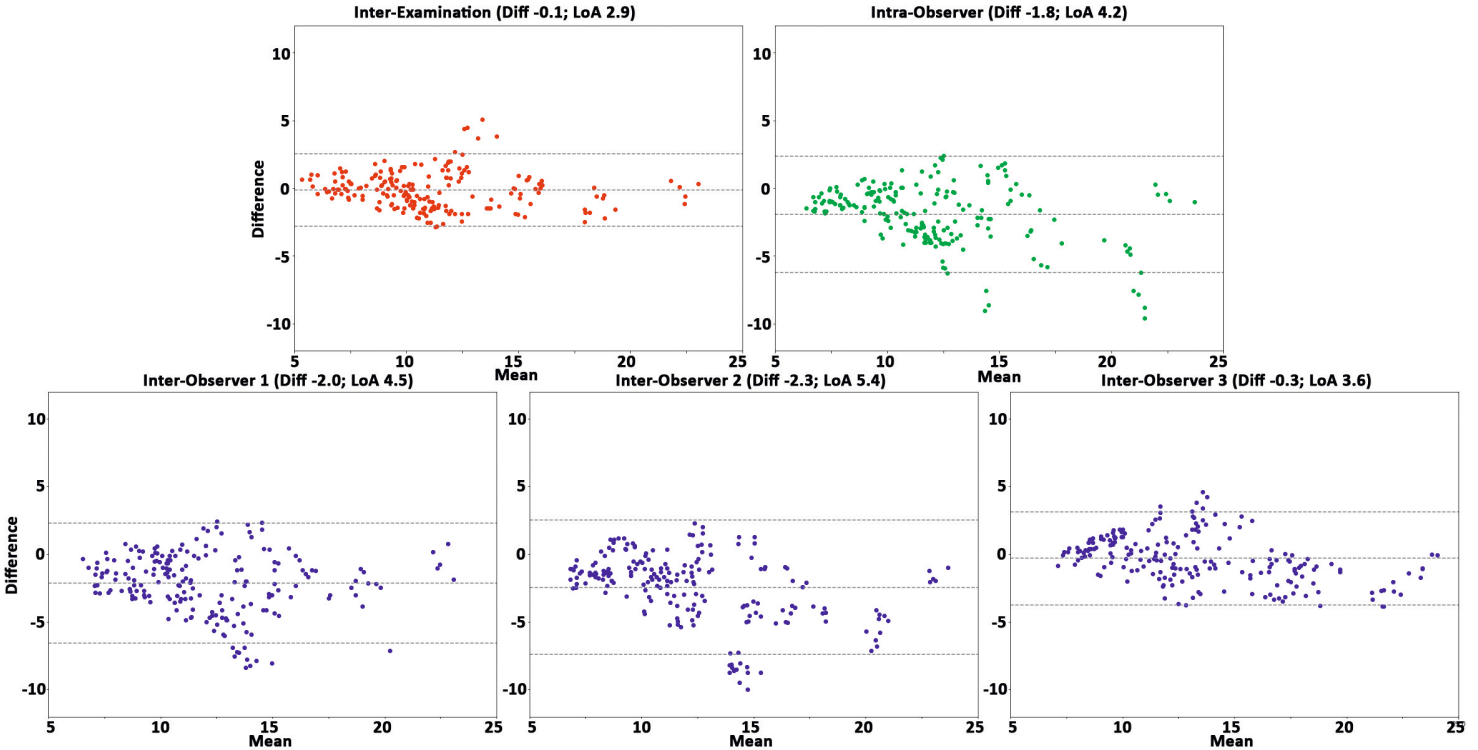

FIGURE 2. The Bland–Altman plots for volume assessment of the interexamination, intraobserver, and interobserver studies. Plots demonstrate the results over all healthy volunteers, anatomical segments, and cardiac phases (n = 250). The plots display volume differences against volume means in mL. Horizontal lines show mean difference (Diff, solid line) and the limits of agreement (LoA, dashed lines).

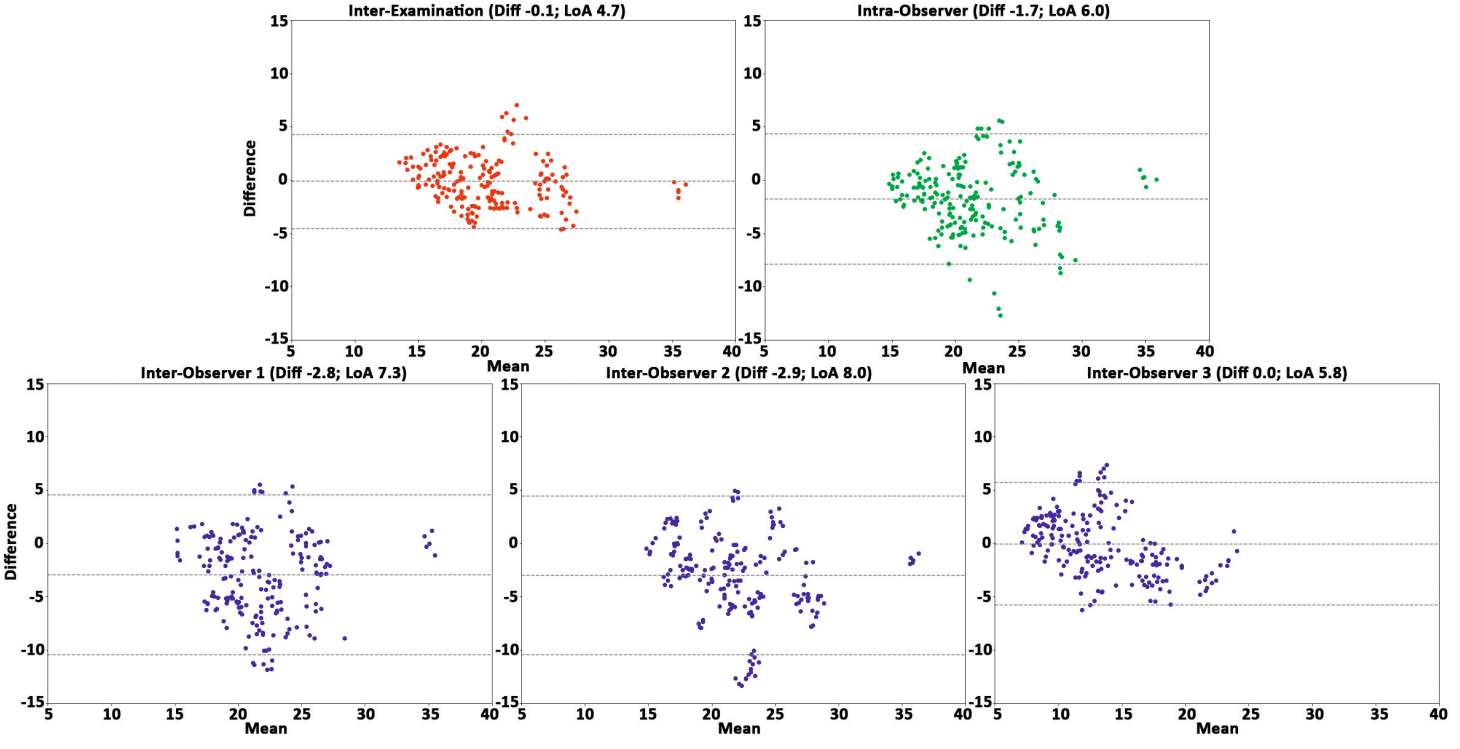

FIGURE 3. The Bland–Altman plots for surface area assessment of the interexamination, intraobserver, and interobserver studies. Plots demonstrate the results over all healthy volunteers, anatomical segments, and cardiac phases (n = 250). Displayed on the vertical and horizontal axis, the difference and means, respectively, in mm2. Horizontal lines show the mean difference (Diff, solid line) and the limits of agreement (LoA, dashed lines).

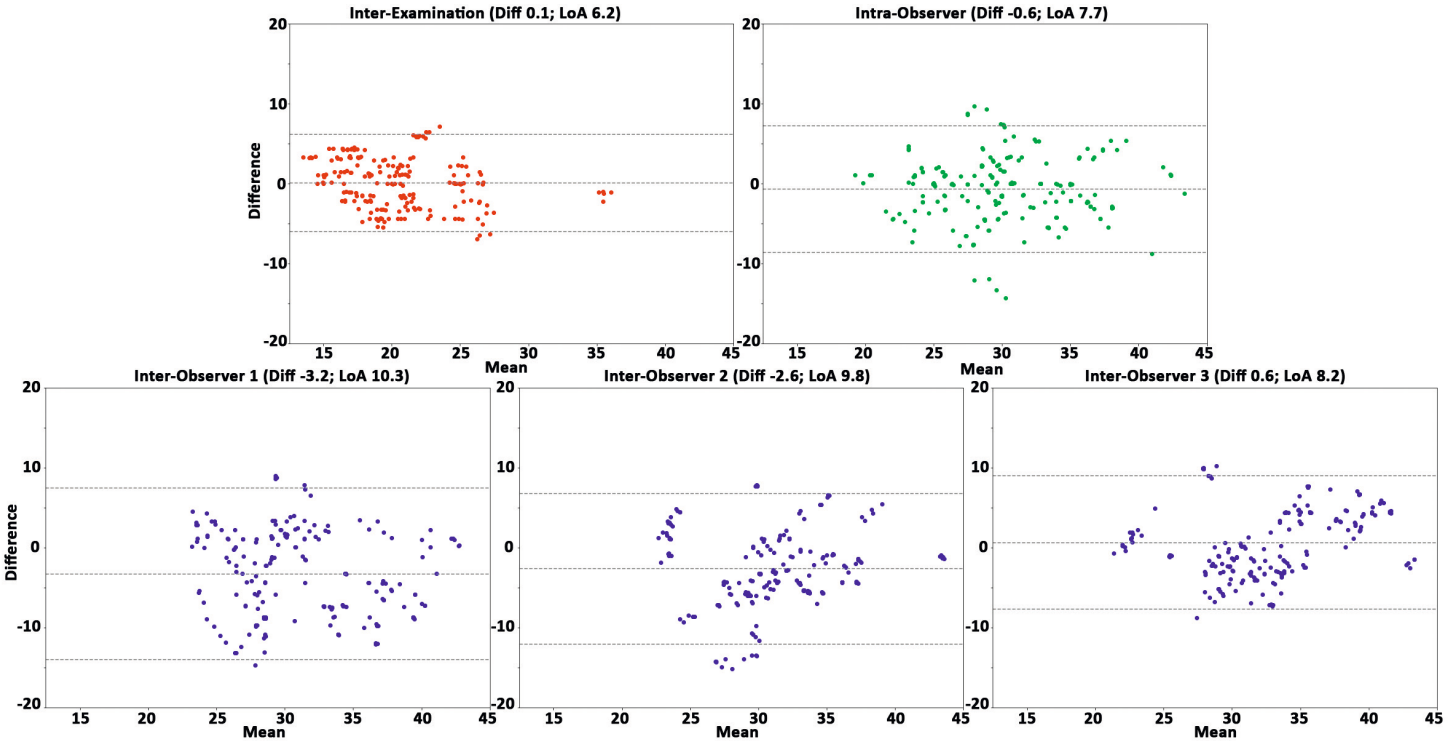

FIGURE 4. The Bland–Altman plots for centerline length assessment over the interexamination, intraobserver, and interobserver studies. Plots demonstrate the results of all healthy volunteers, anatomical segments, and cardiac phases (n = 250). Displayed on the vertical and horizontal axis, the difference and means, respectively, in mm. Horizontal lines show the mean difference (Diff, solid line) and the limits of agreement (LoA, dashed lines).

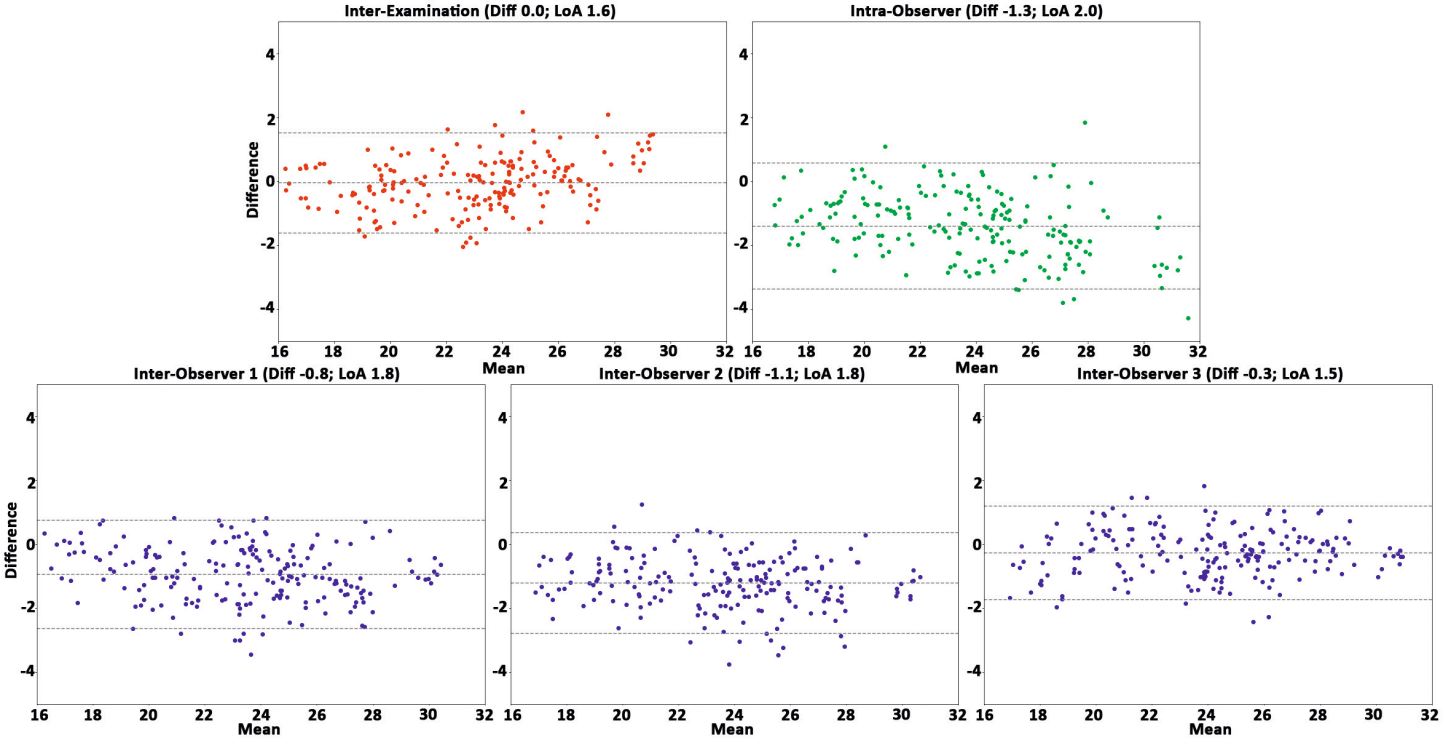

FIGURE 5. The Bland–Altman plots for the maximal diameter assessment the interexamination, intraobserver, and interobserver studies. Plots demonstrate the results over all healthy volunteers, anatomical segments, and cardiac phases (n = 250). Displayed on the vertical and horizontal axis, the difference and means, respectively, in mm. Horizontal lines show the mean difference (Diff, solid line) and the limits of agreement (LoA, dashed lines).

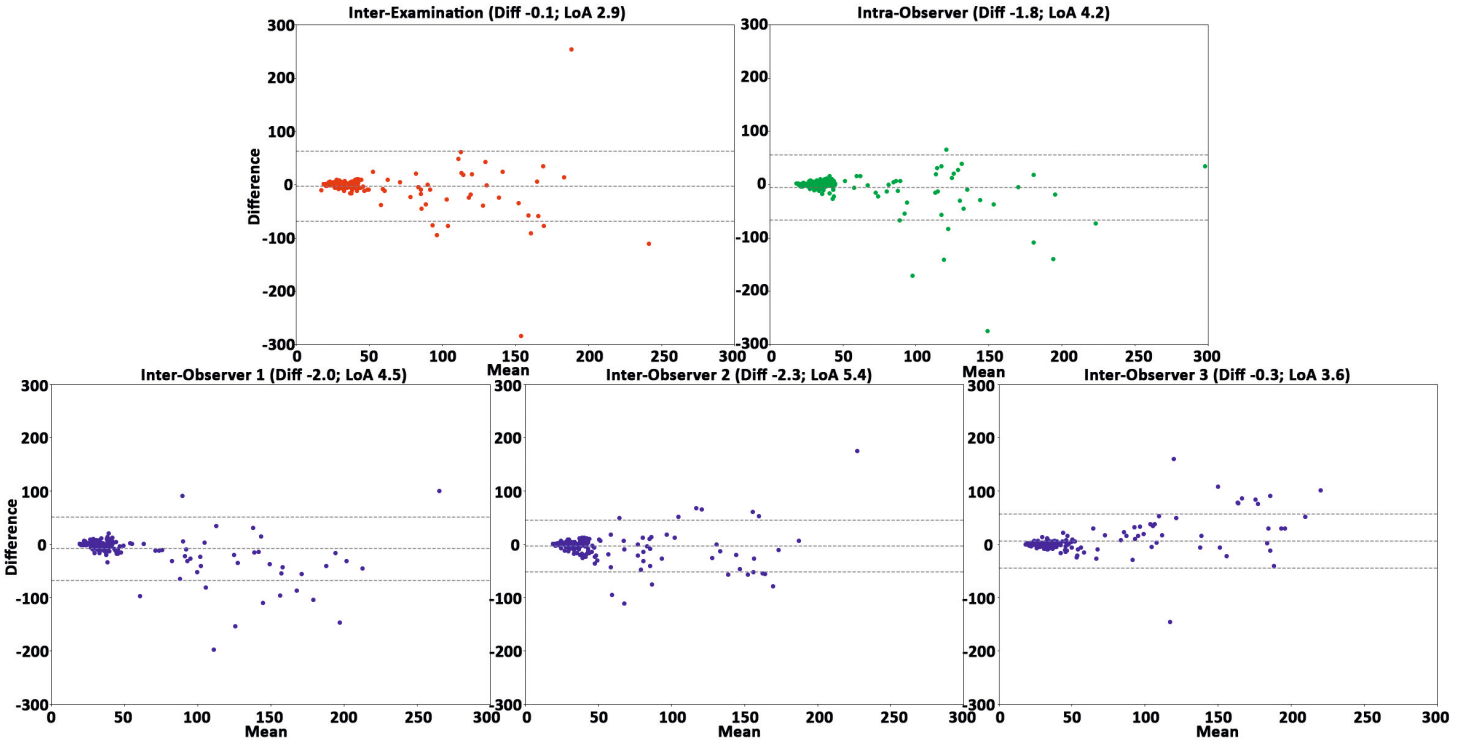

FIGURE 6. The Bland–Altman plots for the curvature radius assessment of the interexamination, intraobserver, and interobserver studies. Plots demonstrate the results over all healthy volunteers, anatomical segments, and cardiac phases (n = 250). Displayed, on the vertical and horizontal axis, the difference and means, respectively, in mm. Horizontal lines show the mean difference (Diff, solid line) and the limits of agreement (LoA, dashed lines).

Table 4. The inter-examination, inter-observer reproducibility and intra-observer repeatability results of the healthy cohort.

	Bland–Altman			Pearson correlation		
Study	**Mean Diff**	**LoA**	**COV [%]**	**r**	**p**	**ICC**
Volume [cm^3 = mL]						
IE–E	-0.1	2.9	13	0.92	<0.01	0.96
IA–O	-1.8	4.2	17	0.85	<0.01	0.86
IE–O1	-2.0	4.5	18	0.80	<0.01	0.82
IE-O2	-2.3	5.4	21	0.78	<0.01	0.79
IE-O3	-0.3	3.6	13	0.92	<0.01	0.95
Surface Area [cm^2]						
IE–E	-0.1	4.7	11	0.86	<0.01	0.92
IA–O	-1.7	6.0	14	0.75	<0.01	0.82
IE–O1	-2.8	7.3	16	0.61	<0.01	0.66
IE-O2	-2.9	8.0	18	0.62	<0.01	0.68
IE-O3	0.0	5.8	12	0.80	<0.01	0.88
Centerline Length [mm]						
IE–E	0.1	6.2	10	0.84	<0.01	0.91
IA–O	-0.6	7.7	13	0.73	<0.01	0.84
IE–O1	-3.2	10.3	16	0.60	<0.01	0.68
IE-O2	-2.6	9.8	16	0.54	<0.01	0.65
IE-O3	0.6	8.2	13	0.74	<0.01	0.83
Maximal Diameter [mm]						
IE–E	0.0	1.6	3	0.97	<0.01	0.98
IA–O	-1.3	2.0	4	0.96	<0.01	0.94
IE–O1	-0.8	1.8	4	0.96	<0.01	0.97
IE-O2	-1.1	1.8	4	0.96	<0.01	0.95
IE-O3	-0.3	1.5	3	0.97	<0.01	0.99
Curvature Radius [mm]						
IE–E	-3.4	59.9	62	0.73	<0.01	0.84
IA–O	-4.7	56.0	57	0.80	<0.01	0.87
IE–O1	-7.6	54.9	55	0.82	<0.01	0.88
IE-O2	-3.4	44.5	46	0.82	<0.01	0.90
IE-O3	4.2	46.0	44	0.89	<0.01	0.92

Results are presented over all healthy volunteers, cardiac phases and anatomical segments (n=250). Abbreviations: Mean Diff – mean difference, LoA – limits of agreement (1.96 * standard deviation mean difference), COV – coefficient of covariance, r –Pearson correlation coefficient, p – probability value, ICC – intra-class correlation coefficient, IE-E – inter-examination, IE-O – inter-observer, IA-O – intra-observer.

Table 5. The inter-observer reproducibility results of the clinical cohort.

Study	Bland–Altman		COV [%]	Pearson correlation		ICC
	Mean Diff	LoA		r	p	
Volume [cm^3 = mL]						
IE–O1	-1.0	5.9	12	0.98	<0.01	0.99
IE-O2	1.2	14.9	32	0.89	<0.01	0.94
IE-O3	2.2	14.2	30	0.89	<0.01	0.94
Surface Area [cm^2]						
IE–O1	-3.3	11.1	16	0.95	<0.01	0.96
IE-O2	-0.6	18.9	29	0.83	<0.01	0.90
IE-O3	2.7	14.2	21	0.89	<0.01	0.93
Centerline Length [mm]						
IE–O1	-0.6	8.8	10	0.94	<0.01	0.97
IE-O2	2.0	13.1	16	0.87	<0.01	0.91
IE-O3	2.6	11.9	15	0.88	<0.01	0.92
Maximal Diameter [mm]						
IE–O1	-0.2	2.5	4	0.98	<0.01	0.99
IE-O2	0.1	5.1	8	0.93	<0.01	0.96
IE-O3	0.3	5.4	8	0.93	<0.01	0.96
Curvature Radius [mm]						
IE–O1	-0.9	31.1	25	0.95	<0.01	0.97
IE-O2	4.3	48.1	40	0.85	<0.01	0.90
IE-O3	5.2	53.6	44	0.84	<0.01	0.89

Results are presented over all subjects, cardiac phases and anatomical segments (n = 150). Abbreviations: Mean Diff –mean difference, Limits of agreement – ±1.96 * standard deviation mean difference, COV – coefficient of covariance, r –correlation coefficient, p – probability value, ICC – intra-class correlation coefficient.

The reproducibility results of the current study demonstrated no major limitations for the (semi-)automatic aortic lumen segmentation of 4D flow MRI. However, some segmentation variability was observed that will affect the reproducibility and repeatability of flow-derived parameters (eg, quantification of kinetic energy for a specific volume [26]). The Bland–Altman plots demonstrated consistent differences over a range of values for all morphometric parameters except for the curvature radius. In order to obtain the smallest relative error, it is recommended that aortic morphometrics and flow derived parameters are derived over a large anatomical segment.

However, for the clinical cohort slightly larger, but still acceptable, LoAs were observed compared to the healthy cohort. For patients and older subjects, more vessel irregularity, complex flow patterns, heart rate variance, and breathing variance is expected compared to healthy volunteers and young subjects. These clinical cohort

characteristics potentially reduce the velocity-to-noise of the 4D flow MRI, which possibly decreased the reproducibility. But, with the use of a multiple-velocity-encoding and highly accelerated sequences, the velocity-to-noise of the 4D flow MRI can potentially be improved and possibly improves the segmentation reproducibility [27-29].

Furthermore, for the healthy and clinical cohort the Bland–Altman analysis demonstrated that the interexamination, interobserver, and intraobserver LoAs for the maximal diameter were 1.5–2.0 mm and 2.4–5.8 mm, respectively. These LoAs for the clinical cohort were below the spatial resolution of the 4D flow MRI. Due to variation in manually repeated measurements of maximal aortic diameters, the European Society of Cardiology considers a change in maximal aortic diameter larger than 5 mm as significant [14]. Hence, the image analysis method for deriving maximal lumen diameter used in this study could have the potential to describe patient characteristics and would be beneficial for the clinical follow-up of patients with pathological aorta diameters, like aneurysms or coarctations.

The low LoAs for the maximal diameter, especially in the healthy cohorts, is presumably driven by the automatic diameter analysis utilized in this study, which determines the maximal diameter over an anatomical segment by constructing a perpendicular plane every millimeter along the segmentation's centerline. The automatic analysis is less influenced by the observer than the manual measurement method, where the observer potentially chooses different measurement locations and plane obliquity towards the vessel [15]. Eventually, both intra- and interobserver variability may potentially be removed by the application of a fully automated 4D flow MRI segmentation method, although interexamination variability would remain [25, 30]. However, these applications are currently only able to create a single segmentation from a time-averaged 4D flow MRI. For moving and stretching vessels (eg, ascending aorta), these time-averaged segmentations can have a misalignment between the segmentation and actual lumen border for specific phases. This misalignment could potentially be problematic when calculating time-specific patient flow properties.

When analyzing the healthy cohort results per anatomical segment, it was observed that the volume, surface area, and centerline length reproducibility was decreased for the pAAo. This may be explained by the minimal anatomic landmark information recorded within the 4D flow MRI, resulting in difficulties in positioning the most proximal plane at the sinotubular junction (10). The reduced pAAo reproducibility may also be explained by the pronounced longitudinal stretching and movement of the ascending aorta during systole compared to the aortic arch and descending aorta (23,31,32). A decreased reproducibility was also observed for the dDAo curvature radius. This may be explained by the minimal longitudinal bending of the dDAo, resulting in instabilities when trying to fit a circle to a nearly straight centerline. This reasoning is supported by

the considerably larger curvature radii observed in dDAo and the Bland–Altman plots, which demonstrate higher differences for larger radii.

Limitations

This study incorporated a healthy volunteer and clinical cohort of only ten and six subjects, respectively. The relatively larger group of healthy volunteers in the study population has probably a less varying heart rate and breathing pattern, which presumably contributed to a better image quality compared to clinical patients. The cohorts, including the subgroups, also had a relatively small age range. Also, only two types of patients with pathological aortas were evaluated, excluding the possibility of verifying the segmentation reproducibility in other pathological aortas.

However, the thoracic aorta lumen was segmented by three observers for five cardiac phases and then partitioned into five anatomical segments, which resulted in a total of 1700 aortic lumen segments, which improved the robustness of the study.

CONCLUSION

This study demonstrated no major reproducibility and repeatability limitations for 4D flow MRI aortic lumen segmentation.

REFERENCES

1. Stalder, A.F., et al., *Quantitative 2D and 3D phase contrast MRI: optimized analysis of blood flow and vessel wall parameters.* Magnetic resonance in medicine, 2008. **60**(5): p. 1218-1231.
2. Frydrychowicz, A., et al., *Three-dimensional analysis of segmental wall shear stress in the aorta by flow-sensitive four-dimensional-MRI.* Journal of Magnetic Resonance Imaging, 2009. **30**(1): p. 77-84.
3. Petersson, S., P. Dyverfeldt, and T. Ebbers, *Assessment of the accuracy of MRI wall shear stress estimation using numerical simulations.* Journal of Magnetic Resonance Imaging, 2012. **36**(1): p. 128-138.
4. Davies, P.F., *Hemodynamic shear stress and the endothelium in cardiovascular pathophysiology.* Nature Clinical Practice Cardiovascular Medicine, 2009. **6**(1): p. 16-26.
5. Boussel, L., et al., *Aneurysm growth occurs at region of low wall shear stress: patient-specific correlation of hemodynamics and growth in a longitudinal study.* Stroke, 2008. **39**(11): p. 2997-3002.
6. Dyverfeldt, P., et al., *4D flow cardiovascular magnetic resonance consensus statement.* Journal of Cardiovascular Magnetic Resonance, 2015. **17**(1): p. 72.
7. Bieging, E.T., et al., *In vivo three-dimensional MR wall shear stress estimation in ascending aortic dilatation.* Journal of Magnetic Resonance Imaging, 2011. **33**(3): p. 589-597.
8. Markl, M., W. Wallis, and A. Harloff, *Reproducibility of flow and wall shear stress analysis using flow-sensitive four-dimensional MRI.* Journal of Magnetic Resonance Imaging, 2011. **33**(4): p. 988-994.
9. Van Ooij, P., et al., *Reproducibility and interobserver variability of systolic blood flow velocity and 3D wall shear stress derived from 4D flow MRI in the healthy aorta.* Journal of Magnetic Resonance Imaging, 2016. **43**(1): p. 236-248.
10. van der Palen, R.L.F., et al., *Scan-rescan reproducibility of segmental aortic wall shear stress as assessed by phase-specific segmentation with 4D flow MRI in healthy volunteers.* MAGMA, 2018.
11. Dyverfeldt, P., et al., *Reproducibility of quantitative analysis of aortic 4D flow data.* Journal of Cardiovascular Magnetic Resonance, 2013. **15**(S1): p. P126.
12. Hope, M.D., et al., *MRI hemodynamic markers of progressive bicuspid aortic valve-related aortic disease.* Journal of Magnetic Resonance Imaging, 2014. **40**(1): p. 140-145.
13. Hiratzka, L.F., et al., *2010 ACCF/AHA/AATS/ACR/ASA/SCA/SCAI/SIR/STS/SVM guidelines for the diagnosis and management of patients with thoracic aortic disease.* Journal of the American College of Cardiology, 2010. **55**(14): p. e27-e129.
14. Erbel, R., et al., *2014 ESC Guidelines on the diagnosis and treatment of aortic diseases: Document covering acute and chronic aortic diseases of the thoracic and abdominal aorta of the adult The Task Force for the Diagnosis and Treatment of Aortic Diseases of the European Society of Cardiology (ESC).* European heart journal, 2014. **35**(41): p. 2873-2926.
15. Elefteriades, J.A. and E.A. Farkas, *Thoracic aortic aneurysm clinically pertinent controversies and uncertainties.* J Am Coll Cardiol, 2010. **55**(9): p. 841-57.
16. Jones, E., T. Oliphant, and P. Peterson, *{SciPy}: Open source scientific tools for {Python}.* 2014.
17. Van Der Walt, S., S.C. Colbert, and G. Varoquaux, *The NumPy array: a structure for efficient numerical computation.* Computing in Science & Engineering, 2011. **13**(2): p. 22.
18. Schroeder, W.J., B. Lorensen, and K. Martin, *The visualization toolkit: an object-oriented approach to 3D graphics*. 2004: Kitware.

19. Antiga, L., et al., *An image-based modeling framework for patient-specific computational hemodynamics.* Medical & biological engineering & computing, 2008. **46**(11): p. 1097.
20. Bland, J.M. and D.G. Altman, *Statistical methods for assessing agreement between two methods of clinical measurement.* lancet, 1986. **1**(8476): p. 307-310.
21. Ghatwary, T., et al., *St George's Vascular Institute Protocol: an accurate and reproducible methodology to enable comprehensive characterization of infrarenal abdominal aortic aneurysm morphology in clinical and research applications.* Journal of Endovascular Therapy, 2012. **19**(3): p. 400-414.
22. Chen, C.-K., et al., *Interobserver and intraobserver variability in measuring the tortuosity of the thoracic aorta on computed tomography.* Journal of vascular surgery, 2018. **68**(4): p. 1183-1192. e1.
23. Bons, L.R., et al., *Intermodality variation of aortic dimensions: How, where and when to measure the ascending aorta.* International journal of cardiology, 2019. **276**: p. 230-235.
24. van Prehn, J., et al., *Intra-and interobserver variability of aortic aneurysm volume measurement with fast CTA postprocessing software.* Journal of Endovascular Therapy, 2008. **15**(5): p. 504-510.
25. Berhane, H., et al., *Fully automated 3D aortic segmentation of 4D flow MRI for hemodynamic analysis using deep learning.* Magnetic resonance in medicine, 2020.
26. Dyverfeldt, P., et al., *Magnetic resonance measurement of turbulent kinetic energy for the estimation of irreversible pressure loss in aortic stenosis.* JACC Cardiovasc Imaging, 2013. **6**(1): p. 64-71.
27. Schnell, S., et al., *Improved assessment of aortic hemodynamics by kt accelerated dual-VENC 4D flow MRI in pediatric patients.* Journal of Cardiovascular Magnetic Resonance, 2016. **18**(1): p. 1-2.
28. Ma, L.E., et al., *Efficient triple-VENC phase-contrast MRI for improved velocity dynamic range.* Magnetic Resonance in Medicine, 2019.
29. Peper, E.S., et al., *Highly accelerated 4D flow cardiovascular magnetic resonance using a pseudo-spiral Cartesian acquisition and compressed sensing reconstruction for carotid flow and wall shear stress.* Journal of Cardiovascular Magnetic Resonance, 2020. **22**(1): p. 1-15.
30. Bustamante, M., et al., *Atlas-based analysis of 4D flow CMR: Automated vessel segmentation and flow quantification.* Journal of Cardiovascular Magnetic Resonance, 2015. **17**(1): p. 87.

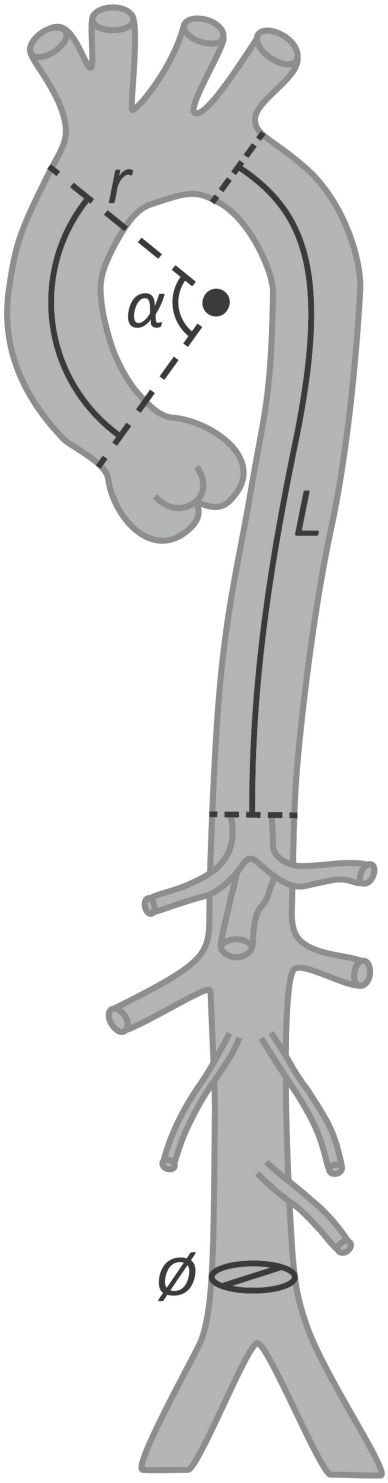
r
α
L
Ø

Appendix to Chapter 2

The accuracy analysis of the in-house developed tool and 4D flow analysis.

INTRODUCTION

The in-house developed software tool to analyze the aorta morphometry was programmed in Python v3.6.4 (Python Software Foundation, Welfeboro Falls, USA) and utilized several open-source scientific libraries: SciPy v.1.1.1 (16), NumPy v1.12.1 (17), Visualization ToolKit v.8.1. (18) and Vascular Modeling ToolKit v1.4.0 (19). To assess the inaccuracy of this software tool and 4D flow MRI analysis, a simulated phantom segmentation and 4D flow MRI phantom data were incorporated as a reference respectively. From a U-shaped phantom blueprint including a distal narrowing (Appendix Figure 1), a simulated phantom segmentation and an MRI-compatible flow phantom were created.

MATERIALS AND METHODS

The simulated phantom segmentation was directly analyzed with the in-house developed software. By manually placing anatomical planes the phantom lumen was divided into five consecutive segments: the inlet tube, U-bend, proximal outlet tube, stenosis tube and the distal outlet tube (Appendix Figure 1).

The MRI-compatible flow phantom (Materialise, Leuven, Belgium) was submerged in a tank filled with a combined gadobutrol (Gadovist®, Bayer Pharma, Berlin, Germany) and gelatin composition to increase signal intensity. The exact composition consisted of 9.9 L water, 600 g gelatin, 100 mL paraben and 1.5 mL gadobutrol. The composition was circulated through the phantom using a stationary pump (AQUA F 10 L, Fiamma, Varese, Italy) with two different settings to assess the effect of different velocities. The U-shaped phantom was scanned in a sagittal imaging direction, resulting in parallel planes towards the legs of the phantom respectively (Appendix Figure 1). The acquisition settings were; (1) flow rate 4.5 L/min, VENC 70 cm/s. (2) flow rate 5.7 L/min, VENC 120 cm/s. None of the acquired 4D flow MRI data sets was subject to phase-wrapping.

The 4D flow MRI was acquired using retrospective electrocardiographic gating with a simulated heart rate of 60 bpm. Sequence parameters were as follows: acquisition spatial resolution: 1.5 × 1.5 × 1.5 mm^3, reconstruction spatial resolution: 0.7 x 0.7 x 1.5 mm^3, temporal resolution: 33-50 ms (28 – 30 phases), echo time/repetition time: 2.3–2.5 ms/4.0–4.3 ms, flip angle: 7°, field of view: 180 × 180 × 40.5 mm^3, turbo field echo factor: 2, sensitivity encoding factor 2 in anterior–posterior direction. Concomitant gradient correction and local phase correction were performed from standard available scanner software.

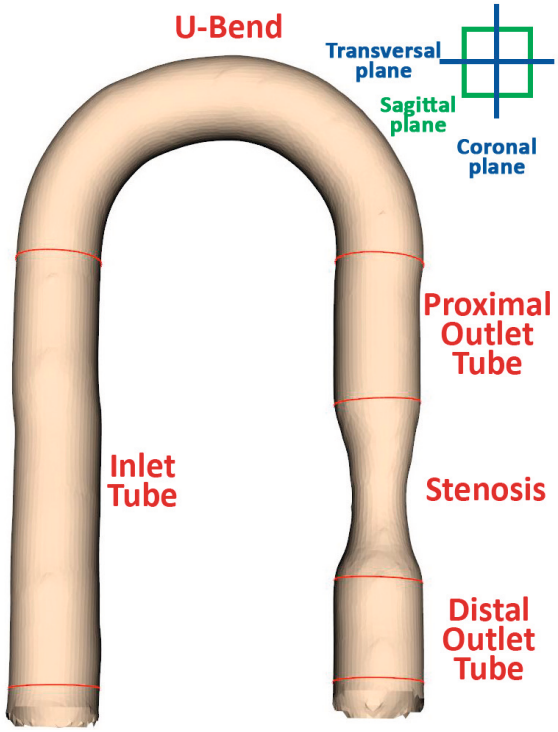

Appendix Figure 1. The phantom lumen partitioning

Next, the phantom 4D flow MRI data was semi-automatically segmented by a single observer (JJ) utilizing CAAS MR Solutions v5.0 (Pie Medical Imaging, Maastricht, The Netherlands). By manually placing start and end points in the phantom, automatically a lumen segmentation was created which subsequently manually was improved.

The phantom segmentation was analyzed with the in-house developed software for the same five segments used for the synthesized phantom segmentation. From the simulated and 4D flow MRI phantom segmentation, the morphometric parameters were computed for each anatomical segment by the in-house developed software. To assess the inaccuracy of the in-house developed software and 4D flow MRI analysis the relative error was determined (calculated as the mismatch between the observed value and true value divided by the true valve, and expressed as percentage). For volume and surface area, this calculation was implemented using the computed centerline length and the true diameter of each segment. The relative error was classified as: very low (≤5%), low (6-10%), intermediate (11–20%), high (21–30%) and very high (>30%).

RESULTS

The simulated phantom segmentation inaccuracy analysis with the in-house developed software tool showed a very low relative error for all parameters, see Appendix Table 1. Between the two segmentations comparable inaccuracies were found over all five segments, the analysis revealed very low relative errors for all parameters, except for volume, which showed a low relative error (volume: 5.7 – 6.2%, surface area: 2.9 – 3.2%, mean diameter: 2.8 – 2.9%, maximal diameter: 3.6 – 4.1% and curvature: -1.2 – 0.0%). Furthermore, the 4D flow MRI segmentation analysis demonstrated for most parameters an overestimation of the blueprint dimensions, see Appendix Table 1.

When analyzing the separate anatomical segments, comparable results were found for most morphometric parameters, see Appendix Table 2. Only in the U-bend segment an increased inaccuracy was found for the volume and surface area, demonstrating an intermediate-to-low relative errors (volume 10.5 – 13.5% and surface area 7.0 – 10.0%).

DISCUSSION

The phantom analysis demonstrated that the in-house developed software tool derived the morphometric parameters from the simulated phantom segmentation with a very low relative error, even while the phantom's lumen was manually partitioned in multiple anatomical segments. Additionally, the MRI-compatible flow phantom analysis also demonstrated that the 4D flow MRI segmentation matched the phantom's blueprint mostly with a very low relatively. This demonstrated a low inaccuracy for semi-automatic lumen segmentation. However, the segmentation and partitioning of the phantom lumen is easier to perform compared to a human aorta, due to the regular shape and clear geometry transitions of the phantom. Therefore, larger observer errors were expected during the image analysis of a human 4D flow MRI compared to the phantom 4D flow MRI.

CONCLUSION

The phantom analysis demonstrated a very-low inaccuracy for both the in-house developed software tool and the 4D flow MRI analysis for the morphometry quantification.

Appendix Table 1. The phantom accuracy results over all five segments, presented as percentage of the mismatch divided by the true value.

Seg	Pump Setting	Volume [%]	Surface Area [%]	Mean Diameter [%]	Max Diameter [%]	Curvature Radius [%]
Syn	x	0.0 [0.0 – 0.0]	0.0 [0.0 – 0.0]	0.0 [0.0 – 0.0]	0.0 [0.0 – 0.0]	0.0
4D flow MRI	Low	5.7 [4.1 – 6.8]	2.9 [2.2 – 3.5]	2.9 [2.2 – 3.3]	4.1 [3.1 – 4.1]	-1.2
	High	6.2 [5.5 – 6.8]	3.2 [2.8 – 3.4]	2.8 [0.1 – 3.1]	3.6 [3.4 – 4.3]	0.0

Data presented as percentage of the mismatch between the observed value and true value divided by the true valve, and expressed as percentage, over all segments (n=5) and notated as the median, lower and upper quartile (median [lower quartile – upper quartile). Abbreviations: Syn – synthetically constructed phantom, and x – not applicable.

Appendix Table 2. The phantom accuracy results per segment.

Pump Setting	Volume [%]	Surface Area [%]	Mean Diameter [%]	Max Diameter [%]	Curvature Radius [%]
Inlet Tube					
Low	5.7	2.9	2.8	5.6	
High	6.8	3.4	0.1	4.5	
U-Bend					
Low	13.5	10.0	3.3	4.1	-1.2
High	10.5	7.0	3.3	4.3	0.0
Proximal Outlet Tube					
Low	4.1	2.2	2.2	3.1	
High	5.5	2.8	2.8	3.5	
Stenosis					
Low	0.2	0.8	-1.6	-0.4	
High	-3.6	-0.8	-3.4	-0.4	
Distal Outlet Tube					
Low	6.8	3.5	3.3	4.1	
High	6.2	3.2	3.1	3.4	

Data presented as percentage of the mismatch between the observed value and true value divided by the true valve, and expressed as percentage

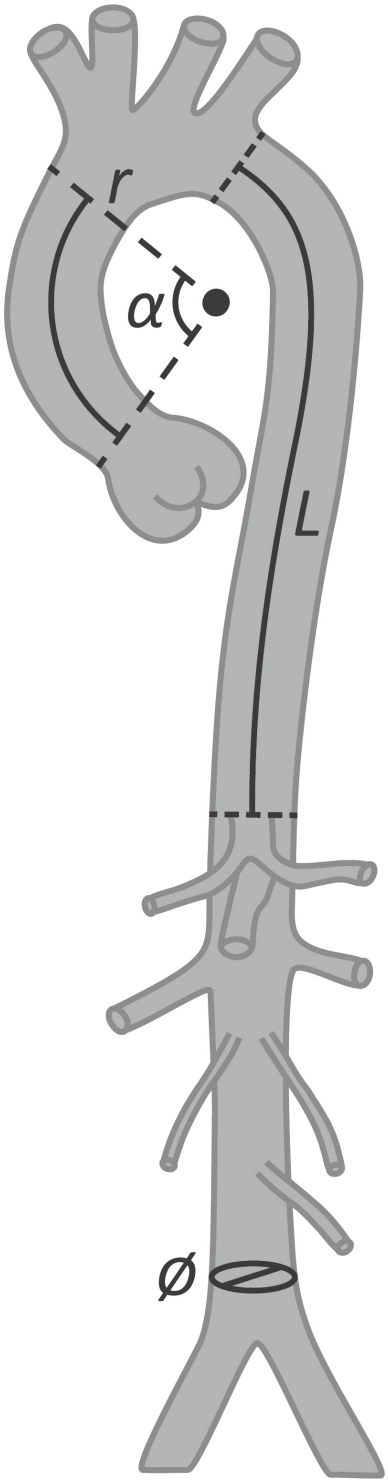
r
α
L
Ø

Supplemental Tables to Chapter 2

Supplemental Table S1. The inter-examination reproducibility results of the healthy cohort per anatomical segment.

	Bland–Altman			Pearson correlation		
Seg	**Mean Diff**	**LoA**	**COV [%]**	**r**	**p**	**ICC**
Volume [cm^3 = mL]						
pAAo	0.4	3.9	15	0.81	<0.01	0.90
dAAo	-0.7	3.4	13	0.89	<0.01	0.92
AoA	0.3	2.4	10	0.96	<0.01	0.98
pDAo	-0.2	2.3	11	0.90	<0.01	0.95
dDAo	-0.4	1.6	9	0.94	<0.01	0.96
Surface Area [cm^2]						
pAAo	0.9	6.2	14	0.66	<0.01	0.79
dAAo	-1.0	4.9	12	0.84	<0.01	0.89
AoA	0.4	3.7	8	0.95	<0.01	0.97
pDAo	-0.2	3.9	9	0.89	<0.01	0.94
dDAo	-0.5	3.0	8	0.88	<0.01	0.92
Centerline Length [mm]						
pAAo	1.4	7.8	14	0.42	<0.01	0.56
dAAo	-1.3	5.7	11	0.75	<0.01	0.83
AoA	0.7	5.0	8	0.91	<0.01	0.95
pDAo	0.0	5.4	8	0.90	<0.01	0.95
dDAo	-0.5	5.3	8	0.77	<0.01	0.87
Maximal Diameter [mm]						
pAAo	0.0	1.6	3	0.92	<0.01	0.96
dAAo	0.0	1.5	3	0.93	<0.01	0.96
AoA	0.2	1.6	3	0.91	<0.01	0.95
pDAo	-0.1	1.8	4	0.86	<0.01	0.93
dDAo	-0.1	1.4	4	0.95	<0.01	0.97
Curvature Radius [mm]						
pAAo	0.7	9.2	14	0.72	<0.01	0.83
dAAo	-1.3	10.8	15	0.79	<0.01	0.88
AoA	0.9	7.8	14	0.86	<0.01	0.92
pDAo	-2.7	13.7	22	0.76	<0.01	0.75
dDAo	-14.4	130.9	58	0.20	0.161	0.33

Data presented over all healthy volunteers and cardiac phases (n=50). Abbreviations: Mean Diff –mean difference, Limits of agreement – ±1.96 * standard deviation mean difference, COV – coefficient of covariance, r –correlation coefficient, p – probability value, ICC – intra-class correlation coefficient, pAAo – proximal ascending aorta, dAAo – distal ascending aorta, AoA – Aortic arch, pDAo – proximal descending aorta and dDAo – distal descending aorta.

Supplemental Table S2. The inter-observer reproducibility results of the healthy cohort per anatomical segment.

		Bland–Altman			Pearson correlation		
Seg	**Analysis**	**Mean Diff**	**LoA**	**COV [%]**	**r**	**p**	**ICC**
Volume [cm^3 = mL]							
pAAo	1	-1.4	5.1	18	0.69	<0.01	0.78
	2	-3.1	6.1	21	0.59	<0.01	0.59
	3	-1.7	2.3	7	0.95	<0.01	0.91
dAAo	1	-3.4	5.2	18	0.63	<0.01	0.57
	2	-5.3	4.9	16	0.71	<0.01	0.46
	3	-1.9	2.2	6	0.95	<0.01	0.89
AoA	1	-0.2	2.8	11	0.94	<0.01	0.97
	2	-0.2	3.1	12	0.95	<0.01	0.97
	3	0.0	2.4	9	0.97	<0.01	0.98
pDAo	1	-2.5	3.5	15	0.79	<0.01	0.71
	2	-0.9	3.4	16	0.76	<0.01	0.82
	3	1.6	2.8	12	0.87	<0.01	0.83
dDAo	1	-2.5	2.2	13	0.89	<0.01	0.70
	2	-1.9	2.0	11	0.89	<0.01	0.77
	3	0.6	1.2	11	0.87	<0.01	0.91
Surface Area [cm^2]							
pAAo	1	-1.6	7.2	16	0.50	<0.01	0.63
	2	-4.1	8.0	17	0.41	<0.01	0.41
	3	-2.5	3.3	7	0.89	<0.01	0.84
dAAo	1	-4.5	7.9	18	0.33	0.018	0.31
	2	-7.2	7.1	15	0.49	<0.01	0.28
	3	-2.7	3.1	6	0.90	<0.01	0.82
AoA	1	0.9	4.3	10	0.92	<0.01	0.95
	2	0.8	4.3	10	0.94	<0.01	0.96
	3	-0.1	3.5	8	0.96	<0.01	0.98
pDAo	1	-4.0	5.7	12	0.73	<0.01	0.64
	2	-1.0	5.8	13	0.70	<0.01	0.79
	3	3.0	4.3	9	0.80	<0.01	0.73
dDAo	1	-4.9	3.7	9	0.80	<0.01	0.49
	2	-2.8	3.3	8	0.87	<0.01	0.75
	3	2.1	3.9	6	0.81	<0.01	0.80

Supplemental Table S2. *Continued*

		Bland–Altman			Pearson correlation		
Seg	Analysis	Mean Diff	LoA	COV [%]	r	p	ICC
Centerline Length [mm]							
pAAo	1	-1.4	8.8	15	0.15	0.30	0.24
	2	-4.5	8.5	14	0.22	0.13	0.20
	3	-3.0	4.6	7	0.66	<0.01	0.59
dAAo	1	-4.6	9.7	18	-0.17	0.23	-0.19
	2	-7.6	8.5	15	0.11	0.43	0.06
	3	-3.0	3.6	6	0.78	<0.01	0.66
AoA	1	2.5	5.8	10	0.86	<0.01	0.88
	2	2.2	5.4	9	0.91	<0.01	0.91
	3	-0.3	4.3	8	0.95	<0.01	0.97
pDAo	1	-5.0	8.0	11	0.73	<0.01	0.62
	2	-0.5	8.5	13	0.69	<0.01	0.79
	3	4.5	5.3	7	0.80	<0.01	0.66
dDAo	1	-7.5	5.2	8	0.74	<0.01	0.39
	2	-2.7	4.6	7	0.89	<0.01	0.84
	3	4.8	5.2	7	0.86	<0.01	0.67
Maximal Diameter [mm]							
pAAo	1	-0.8	1.9	4	0.90	<0.01	0.92
	2	-1.3	2.1	4	0.86	<0.01	0.84
	3	-0.5	1.6	3	0.93	<0.01	0.95
dAAo	1	-1.0	1.7	3	0.91	<0.01	0.90
	2	-1.3	1.7	3	0.91	<0.01	0.86
	3	-0.3	1.0	2	0.97	<0.01	0.98
AoA	1	-0.9	1.6	3	0.91	<0.01	0.90
	2	-1.1	1.6	3	0.91	<0.01	0.87
	3	-0.2	1.3	3	0.93	<0.01	0.96
pDAo	1	-0.8	2.1	5	0.84	<0.01	0.86
	2	-0.7	1.7	4	0.90	<0.01	0.92
	3	0.2	1.8	4	0.89	<0.01	0.94
dDAo	1	-0.5	1.5	4	0.94	<0.01	0.95
	2	-1.1	1.4	4	0.94	<0.01	0.92
	3	-0.6	1.3	3	0.95	<0.01	0.96

Supplemental Table S2. *Continued*

		Bland–Altman			Pearson correlation		
Seg	**Analysis**	**Mean Diff**	**LoA**	**COV [%]**	**r**	**p**	**ICC**
Curvature Radius [mm]							
pAAo	1	-3.9	17.2	25	0.27	0.06	0.37
	2	-7.4	23.5	34	0.27	0.06	0.28
	3	-3.5	18.2	24	0.64	<0.01	0.73
dAAo	1	-0.7	11.8	15	0.79	<0.01	0.88
	2	-0.2	11.4	16	0.70	<0.01	0.79
	3	0.5	11.2	15	0.77	<0.01	0.82
AoA	1	1.3	9.6	17	0.79	<0.01	0.88
	2	0.0	9.1	16	0.85	<0.01	0.92
	3	-1.3	8.1	14	0.88	<0.01	0.93
pDAo	1	-2.7	11.7	19	0.48	<0.01	0.60
	2	-1.6	11.5	19	0.46	<0.01	0.61
	3	1.1	4.7	7	0.92	<0.01	0.95
dDAo	1	-31.7	108.3	51	0.43	<0.01	0.54
	2	-7.6	94.5	43	0.45	<0.01	0.61
	3	24.1	90.6	36	0.54	<0.01	0.63

Data presented over all healthy volunteers and cardiac phases (n=50). Abbreviations: Mean Diff –mean difference, Limits of agreement – ±1.96 * standard deviation mean difference, COV – coefficient of covariance, r –correlation coefficient, P – probability value, ICC – intra-class correlation coefficient, pAAo – proximal ascending aorta, dAAo – distal ascending aorta, AoA – Aortic arch, pDAo – proximal descending aorta and dDAo – distal descending aorta.

Supplemental Table S3. The intra-observer reproducibility results of the healthy cohort per anatomical segment.

	Bland–Altman			Pearson correlation		
Seg	**Mean Diff**	**LoA**	**COV [%]**	**r**	**p**	**ICC**
Volume [cm^3 = mL]						
pAAo	-2.2	5.5	19	0.72	<0.01	0.75
dAAo	-2.4	4.3	16	0.84	<0.01	0.80
AoA	-0.6	3.2	13	0.93	<0.01	0.96
pDAo	-2.0	4.4	19	0.70	<0.01	0.72
dDAo	-2.0	2.1	11	0.93	<0.01	0.79
Surface Area [cm^2]						
pAAo	-1.0	7.1	16	0.58	<0.01	0.72
dAAo	-2.3	2.9	13	0.76	<0.01	0.79
AoA	0.0	4.8	11	0.90	<0.01	0.95
pDAo	-2.2	7.1	16	0.60	<0.01	0.68
dDAo	-2.8	3.1	8	0.88	<0.01	0.75
Centerline Length [mm]						
pAAo	1.2	7.9	14	0.39	<0.01	0.54
dAAo	-1.4	6.3	12	0.65	<0.01	0.76
AoA	0.9	6.2	10	0.83	<0.01	0.90
pDAo	-1.3	10.0	15	0.53	<0.01	0.64
dDAo	-2.7	4.6	7	0.79	<0.01	0.76
Maximal Diameter [mm]						
pAAo	-2.0	2.0	4	0.90	<0.01	0.78
dAAo	-1.8	1.7	3	0.93	<0.01	0.81
AoA	-0.7	1.7	4	0.91	<0.01	0.92
pDAo	-0.9	1.8	4	0.90	<0.01	0.90
dDAo	-1.2	1.6	4	0.94	<0.01	0.90
Curvature Radius [mm]						
pAAo	-0.1	9.4	15	0.69	<0.01	0.82
dAAo	0.5	12.0	17	0.69	<0.01	0.82
AoA	0.3	7.7	13	0.86	<0.01	0.93
pDAo	-1.8	12.7	21	0.50	<0.01	0.63
dDAo	-22.5	118.0	50	0.39	<0.01	0.53

Data presented over all healthy volunteers and cardiac phases (n=50). Abbreviations: Mean Diff –mean difference, Limits of agreement – ±1.96 * standard deviation mean difference, COV – coefficient of covariance, r –correlation coefficient, P – probability value, ICC – intra-class correlation coefficient, pAAo – proximal ascending aorta, dAAo – distal ascending aorta, AoA – Aortic arch, pDAo – proximal descending aorta and dDAo – distal descending aorta.

Supplemental Table S4. The inter-observer results of the clinical cohort per subgroup.

		Bland–Altman			Pearson correlation		
Population	**Analysis**	**Mean Diff**	**LoA**	**COV [%]**	**r**	**p**	**ICC**
Volume [cm^3 = mL]							
TAA	1	-1.5	8.5	11	0.97	<0.01	0.97
	2	0.5	17.8	24	0.79	<0.01	0.88
	3	2.0	16.0	21	0.78	<0.01	0.87
CoA	1	-1.1	1.5	10	0.97	<0.01	0.96
	2	-0.7	2.0	13	0.95	<0.01	0.96
	3	0.4	2.5	16	0.92	<0.01	0.95
Healthy volunteers	1	-0.5	5.4	10	0.95	<0.01	0.98
	2	3.7	17.6	34	0.94	<0.01	0.67
	3	4.1	17.9	34	0.49	<0.01	0.61
Surface Area [cm^2]							
TAA	1	-2.3	8.3	9	0.95	<0.01	0.94
	2	0.6	16.2	17	0.67	<0.01	0.79
	3	2.9	13.1	14	0.67	<0.01	0.78
CoA	1	-1.6	2.5	8	0.96	<0.01	0.95
	2	-1.3	3.0	9	0.94	<0.01	0.95
	3	0.3	4.1	12	0.89	<0.01	0.94
Healthy volunteers	1	-6.0	16.0	21	0.93	<0.01	0.81
	2	-1.1	28.4	40	0.35	0.01	0.49
	3	4.9	19.6	26	0.35	0.01	0.46
Centerline Length [mm]							
TAA	1	-2.6	9.0	9	0.92	<0.01	0.94
	2	1.4	13.2	14	0.79	<0.01	0.85
	3	4.0	11.2	11	0.89	<0.01	0.87
CoA	1	-1.4	3.9	7	0.96	<0.01	0.96
	2	-1.5	5.0	9	0.93	<0.01	0.95
	3	-0.1	5.9	10	0.90	<0.01	0.95
Healthy volunteers	1	2.2	9.4	10	0.86	<0.01	0.90
	2	6.2	14.3	16	0.67	<0.01	0.70
	3	4.0	15.0	17	0.54	<0.01	0.65

Supplemental Table S4. *Continued*

Population	Analysis	Bland–Altman		COV [%]	Pearson correlation		
		Mean Diff	LoA		r	p	ICC
Maximal Diameter [mm]							
TAA	1	-0.2	2.5	4	0.98	<0.01	0.99
	2	0.1	5.1	8	0.93	<0.01	0.96
	3	0.3	5.4	8	0.93	<0.01	0.96
CoA	1	-0.7	3.1	8	0.93	<0.01	0.95
	2	-0.6	3.6	9	0.90	<0.01	0.93
	3	0.1	2.0	5	0.95	<0.01	0.98
Healthy volunteers	1	-0.9	1.2	2	0.99	<0.01	0.98
	2	0.4	7.8	14	0.63	<0.01	0.76
	3	1.3	8.0	14	0.62	<0.01	0.75
Curvature Radius [mm]							
TAA	1	-1.5	16.7	14	0.97	<0.01	0.98
	2	-0.9	37.5	31	0.85	<0.01	0.92
	3	0.6	0.6	32	0.83	<0.01	0.91
CoA	1	-5.3	43.6	43	0.87	<0.01	0.89
	2	-5.4	26.3	26	0.92	<0.01	0.95
	3	-0.2	46.6	44	0.83	<0.01	0.90
Healthy volunteers	1	4.1	24.2	16	0.98	<0.01	0.99
	2	19.2	59.9	44	0.94	<0.01	0.87
	3	15.1	66.3	50	0.94	<0.01	0.87

Results are presented per subgroup over all cardiac phases and anatomical segments (n=50). Abbreviations: Mean Diff –mean difference, Limits of agreement – ±1.96 * standard deviation mean difference, COV – coefficient of covariance, r –correlation coefficient, p – probability value, ICC – intra-class correlation coefficient.